

Theoretical Investigation of Samarium Hexaboride

**Partha Goswami and Udai Prakash Tyagi*

D.B.College, University of Delhi, Kalkaji, New Delhi-110019, India

**Email of the corresponding author: physicsgoswami@gmail.com*

Email of the second author: uptyagi@yahoo.co.in

Abstract

We investigate the periodic Anderson model of the bulk samarium hexaboride in the slave-boson framework assuming the presence of ferromagnetic impurities. Our analysis provides a strong evidence that the system is in the quantum anomalous Hall phase when the exchange interaction is not zero. Thereafter, we show that the bulk samarium hexaboride is a strong topological insulator calculating Z_2 invariant using the Fu-Kane-Mele formalism.

Keywords: Exchange interaction, Quantum anomalous Hall phase, Periodic Anderson model, Z_2 invariant, Fu-Kane-Mele formalism

1.Introduction

The strong correlation effects and diverse surface conditions make a generic topological Kondo Insulator (TKI)[1-3]system, such as SmB_6 , extremely complicated - almost a Gordian knot. This communication is on SmB_6 —a narrow gap TKI which, with a high-temperature metallic phase, transforms into a paramagnetic charge insulator below 45 K. It has been suggested [1,2], as well as there is mounting evidence [4-6] during the past several years, that SmB_6 is a strong topological insulator. This has generated great deal of excitement in the condensed matter physics community and it still remains a matter of intense debate [7-9]. The supporting evidence for the TKI scenario [4-6] notwithstanding, there is no jury-verdict regarding the nature of the bulk and surface states of SmB_6 [7-9]. In this communication, we show that the compound SmB_6 is a strong topological insulator (STI). This is in disagreement with what had been reported in refs.[7,8].

We consider the slave boson (SB) mean-field-theoretic version of the periodic Anderson model (PAM) [3, 10,11] for a TKI like SmB_6 on a simple cubic lattice with one spin-degenerate orbital per lattice site each for d and f electrons. Assuming the presence of the ferromagnetic magnetic impurities in our system, we introduce exchange interaction (M) in the model Hamiltonian. We obtain the bulk band spectrum and calculate the Chern number to show that the system is in the quantum anomalous Hall (QAH)phase when $M \neq 0$ which corroborates the possibility of three-dimensional quantum anomalous Hall effect in ferromagnetic insulators [12]. We also calculate the Z_2 invariant using the eigenvalues of the space inversion operator with in the Fu-Kane framework [13] for $M = 0$. We obtain $Z_2 = -1$. This shows that the system is a strong topological insulator.

Our minimalistic bulk Hamiltonian captures essential physics TKI in the presence of the coulomb repulsion U_f ($\gg t_{d1}$) between f electrons on the same site, and the spin-orbit hybridization V . There are terms (t_{d1}, t_{f1}) which represent the NN hopping parameter for d and f electrons. The band warping factor, usually associated with the Hamiltonian of a topological insulator, has not been considered here for the mathematical simplicity. There are three parameters (b, λ, ξ) of the SB theory [3]. The method to obtain them is explained clearly in ref. [3]. We never-the-less summarize briefly below to make this article self-contained. The constraint $U_f \gg t_{d1}$ imposes a non-holonomic constraint, viz. the exclusion of the double occupancy, which is very difficult to manipulate. The SB- framework provides a platform to reformulate this nonholonomic constraint into a holonomic constraint that can be implemented with a Lagrange multiplier. Here, an electron annihilation operator is written as the product of a spinless boson creation operator (SB) and a spinful fermion annihilation operator (We represent them by annihilation operators $f_{k,\tau}^\dagger = (b^\dagger c_{k,\tau})$ in momentum space. Here, the index τ ($= \uparrow, \downarrow$) represents the spin.). This basically corresponds to the assumption that the annihilation of an electron is equivalent to simultaneous creation of a slave-bosonic hole and annihilation of a fermionic spinon. In the present SB framework, we make the further assumption that the slave boson field (b) at each lattice site can be replaced by a c -number. The complications associated with the large on-site repulsion ($U_f \gg t_{d1}$) between the f -electrons is conveniently circumvented in the SB theory by imposing the holonomic constraint $\sum_\tau \langle c_\tau^\dagger c_\tau \rangle = 1 - b^2$ at a site to remove the double occupancy. The term $\lambda [\sum_{k,\tau = \uparrow, \downarrow} \langle c_{k,\tau}^\dagger c_{k,\tau} \rangle + N_c (b^2 - 1)]$ (see ref.[3]), where N_c (N_d) is the number of c -fermions (d -fermions) and $N_c = N_d$ required for the formation of Kondo singlet states between d and c fermions at each lattice site, to be added to the system Hamiltonian to enforce the constraint on the pseudo-particles due to the infinite on-site Coulomb repulsion. Therefore, the signature of the assumption “large on-site repulsion ($U_f \gg t_{d1}$) between the f -electrons” is carried over by the parameters λ and b . The constant term $\lambda N_c (b^2 - 1)$ in the Hamiltonian is to be dropped here-in-after as it has no significance in the calculation below. Moreover, we neglected the dynamics of the boson field completely as the light slave boson creation and destruction operators were replaced by a c -number ‘ b ’. This approximation reduced the system to a non-interacting one with the bulk spectral gap dependent on the parameters (λ, b, ξ, V) . Whereas the first two parameters took care of the strong correlation effect between the f -electrons, the hybridization parameter V is the harbinger of a topological dispersion. The term ξ enforces the fact that there are equal number of d and f fermions. In order to have a Kondo insulator, formation of singlet states between d and f fermions is needed at each lattice site. This means that the number of d and f fermions are equal on average. The total parameters are slave-boson field b , auxiliary chemical potentials ξ and μ (μ is a free parameter which will be taken as zero in this article), and the Lagrange multiplier λ . One obtains equations for the parameters (b, λ, ξ) minimizing the thermodynamic potential per unit volume. We find that $\lambda = -6t_{f1} + 6b^2t_{f1}$, and $\xi = -3t_{d1} + 3t_{f1}$. The admissible value of b^2 is 1^- .

The paper is organized as follows: In section 2, we obtain the bulk band spectrum in the slave-boson formalism. Next, we calculate the Chern number to show the strong evidence of the system being in the quantum anomalous Hall (QAH) phase when $M \neq 0$. We obtain the surface state Hamiltonian in section 3. We also calculate the Z_2 invariant using the eigenstates of the space inversion operator within the Fu-Kane-Mele framework [13]. A mystery centers on the existence of the bulk in-gap states of the system. We point out some related issues as a motivation for further investigation in section 4 together with the highlights of the present work. The paper ends with very brief concluding remarks.

2. Chern Number

We consider below extension of the slave boson (SB) mean-field-theoretic version of the periodic Anderson model (PAM) [3,10,11] for a (topological) Kondo insulator on a simple cubic lattice with one spin-degenerate orbital per lattice site each for d and f electrons. The SB protocol has been summarized below. In momentum(\mathbf{k})-space, we represent them by creation (annihilation) operators $d_{\mathbf{k},\tau}^\dagger$ ($d_{\mathbf{k},\tau}$) and $f_{\mathbf{k},\tau}^\dagger = bc_{\mathbf{k},\tau}^\dagger$ ($bc_{\mathbf{k},\tau}$), respectively. Here, the index τ ($= \uparrow, \downarrow$) represents the spin. The Hamiltonian H_{PAM} consists of two parts, namely, the hopping of the individual orbitals, and the hybridization parameter V between d and f orbitals. With these ingredients, on a simple cubic lattice, the momentum-space Hamiltonian given in ref.[3] is as follows:

$$H_{PAM}(b, \lambda, \xi) = \sum_{\mathbf{k}, \tau = \uparrow, \downarrow} \widetilde{E}_k^d(\mu, \xi) d_{\mathbf{k},\tau}^\dagger d_{\mathbf{k},\tau} + \sum_{\mathbf{k}, \tau = \uparrow, \downarrow} \widetilde{E}_k^f(\mu, b, \lambda, \xi) c_{\mathbf{k},\tau}^\dagger c_{\mathbf{k},\tau} + b \sum_{\mathbf{k}, \tau = \uparrow, \downarrow} \{F_{\tau = \uparrow, \downarrow}(k) d_{\mathbf{k},\tau}^\dagger c_{\mathbf{k},\tau} + \text{H.C.}\} + \lambda N_c (b^2 - 1) \quad (1)$$

$$\widetilde{E}_k^d(\mu, k) = -\mu - \xi - [2t_{d1} c_1(k) + 4t_{d2} c_2(k) + 8t_{d3} c_3(k)], \quad (2)$$

$$\widetilde{E}_k^f(\mu, b, k) = -\mu + \xi - b^2 [-\epsilon_f + 2t_{f1} c_1(k) + 4t_{f2} c_2(k) + 8t_{f3} c_3(k)] + \lambda, \quad (3)$$

$$c_1(k) = (\cos k_x a + \cos k_y a + \cos k_z a), \quad \lambda = -6t_{f1} + 6b^2 t_{f1}, \quad \xi = -3t_{d1} + 3t_{f1},$$

$$c_2(k) = (\cos k_x a \cdot \cos k_y a + \cos k_y a \cdot \cos k_z a + \cos k_z a \cdot \cos k_x a),$$

$$c_3(k) = (\cos k_x a \cdot \cos k_y a \cdot \cos k_z a), \quad (4)$$

As one can see from (1), the dispersion of the f -electron is renormalized by λ and its hopping amplitude by b^2 . Moreover, the hybridization amplitude is also renormalized by the c -number b . Since the f - and d -states have different parities, the momentum-dependent form-factor matrix $F_{\tau = \uparrow, \downarrow}(k)$ involved in the third term in (1) must be odd: $F_{\tau = \uparrow, \downarrow}(-k) = -F_{\tau = \uparrow, \downarrow}(k)$. This is required in order to preserve time reversal symmetry (TRS), as the matrix involves coupling with the physical spin of the electron. Therefore, we write $F_{\tau = \uparrow, \downarrow}(k) = 2V(\mathbf{s}(k) \cdot \boldsymbol{\tau}')$, where V is a constant parameter characterizing the spin-orbit hybridization, $\mathbf{s}(k) = (\sin k_x a, \sin k_y a, \sin k_z a)$ and $\boldsymbol{\tau}' =$

(τ_x, τ_y, τ_z) are the Pauli matrices in spin space. The terms (t_{d1}, t_{f1}) , (t_{d2}, t_{f2}) , and (t_{d3}, t_{f3}) , respectively, are the NN , NNN , and $NNNN$ hopping parameters for d and f electrons; ϵ_f is the onsite energy of the f electrons and N_c is the number of lattice sites for these electrons. Furthermore, we assume the presence of the ferromagnetic magnetic impurities (FMI) in the Hamiltonian in (1) under consideration. The impurities are assumed to be interacting with d electrons only. We absorb the magnitude of the impurity spin $|\mathbf{S}| > 1$ into the ferromagnetic coupling constant J and write $M = |J| |\mathbf{S}|$. The system shows the bulk metallic as well as the bulk insulating phases determined by the sign of t_{f1} . It is positive for the former and negative for the latter phase [3]. The negative sign of t_{f1} is also necessary for the band inversion, which induces the topological state [3]. Throughout the paper, we choose t_{d1} to be the unit of energy.

In the basis $(d_{k,\uparrow}^\dagger, d_{k,\downarrow}^\dagger, bc_{k,\uparrow}^\dagger, bc_{k,\downarrow}^\dagger)$, we can write the Hamiltonian matrix corresponding to (1) as

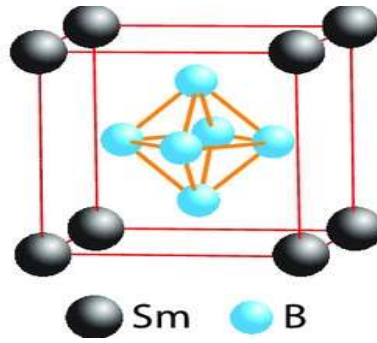
$$h_{PAM}(b, \lambda, \xi) = \frac{\widetilde{E}_k^d(\mu, k)}{2} (\mathbb{I} + \gamma^0) + \frac{\widetilde{E}_k^f(\mu, b, k)}{2} (\mathbb{I} - \gamma^0) + 2C_\mu \Sigma^\mu + \vartheta_\mu \gamma^0 \gamma^\mu. \quad (5)$$

Here \mathbb{I} is the identity matrix, $C_\mu = (0, 0, M)$, $\Sigma^\mu = \left(\frac{1}{2}\right) \epsilon^{\mu\nu\rho} \sigma_{\nu\rho}$, $\sigma_{\nu\rho} = \left(\frac{i}{2}\right) [\gamma_\nu, \gamma_\rho]$, and $\vartheta_\mu = (\vartheta_1, \vartheta_2, \vartheta_3)$. These are $\vartheta_1 = \vartheta_x = (2Vb \sin ak_x)$, $\vartheta_2 = \vartheta_y = (2Vb \sin ak_y)$, and $\vartheta_3 = \vartheta_z = 2Vb$

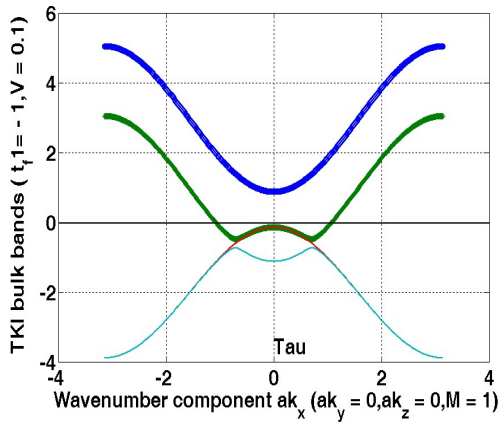
$(\sin ak_z)$, respectively. The Dirac matrices $(\gamma^0, \gamma^1, \gamma^2, \gamma^3, \gamma^5)$ in contravariant notations are $\gamma^0 = \tau^z \otimes I^{2 \times 2}$, $\gamma^j = i\tau^y \otimes \tau^j$, τ^i are Pauli matrices, $j = 1, 2, 3$, and $\gamma^5 = i\gamma^0 \gamma^1 \gamma^2 \gamma^3$. The eigenvalues E_n of the Hamiltonian matrix (5) are given by

$$E_n(s, \tau, k, b, M) = \frac{\widetilde{E}_k^d(\mu, k) + \widetilde{E}_k^f(\mu, b, k) + \tau M}{2} + s \left[\frac{(\widetilde{E}_k^d(\mu, k) - \widetilde{E}_k^f(\mu, b, k) + \tau M)^2}{4} + \vartheta_x^2 + \vartheta_y^2 + \vartheta_z^2 \right]^{1/2} \quad (6)$$

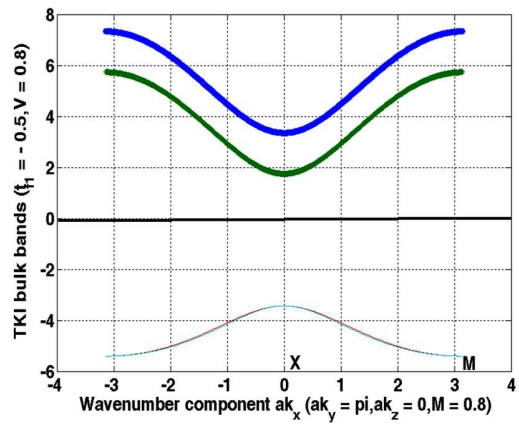
where $n = 1, 2, 3, 4$, $\tau = \pm 1$ is the spin index and $s = \pm 1$ is the band-index. In Figure 1(a), we have shown a diagrammatic representation of SmB_6 crystal structure with cubic lattice constant a ($= 0.413$ nm). The Sm ions are located at the corners and the B_6 octahedron at the center of the cubic lattice. In Figures (b), (c) and (d), we have plotted the bulk band energies of the system in (6) in the insulating phase (where t_{f1} is negative). The high symmetry points (HSPs) of the bulk Brillouin zone (BZ) $\Gamma(0, 0, 0)$, $X(0, \pi, 0)$, $M(\pi, \pi, 0)$, and $R(\pi, \pi, \pi)$ are indicated in these figures. The numerical values of the parameters used in the plots are $t_{d1} = 1$, $t_{f1} = -0.5$ (negative value ensures insulating bulk), $t_{d2} = 0.01$, $t_{f2} = 0.01$, $t_{d3} = 0.001$, $t_{f3} = 0.001$, $\epsilon_f = -0.02$, $V = 0.8$, $b = 0.9899$, $\mu = 0$, and $M \neq 0$. In Figures (e) and (f), however, $M = 0$. The Figures (f) and (g) show metallicity as $t_{f1} > 0$. In Figure (g), $M \neq 0$. We do find that Figure (b) displays avoided crossing. In Figure (h) we have shown 3D representation of all the four bands. All energies in our calculation/graphical representation below are expressed in units of the first neighbor hopping t_{d1} for d -electrons as this corresponds to the kinetic energy of these itinerant electrons and therefore the most dominant.



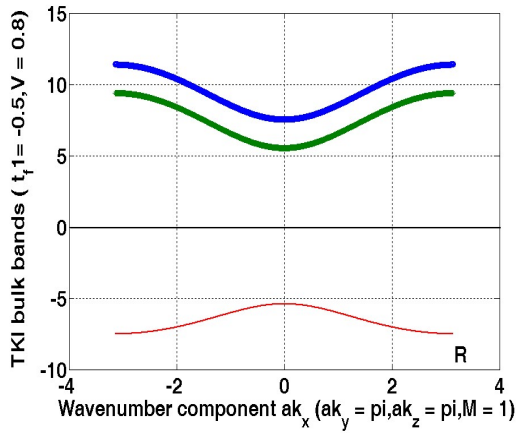
(a)



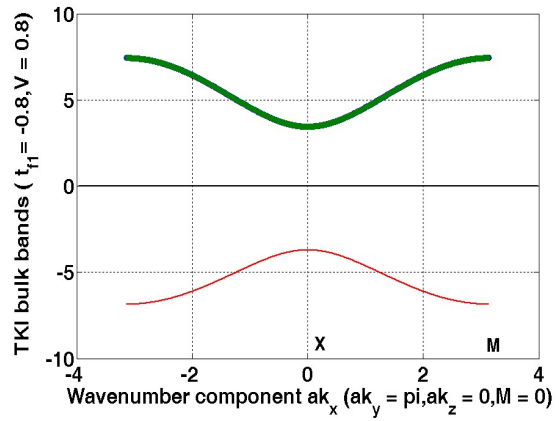
(b)



(c)



(d)



(e)

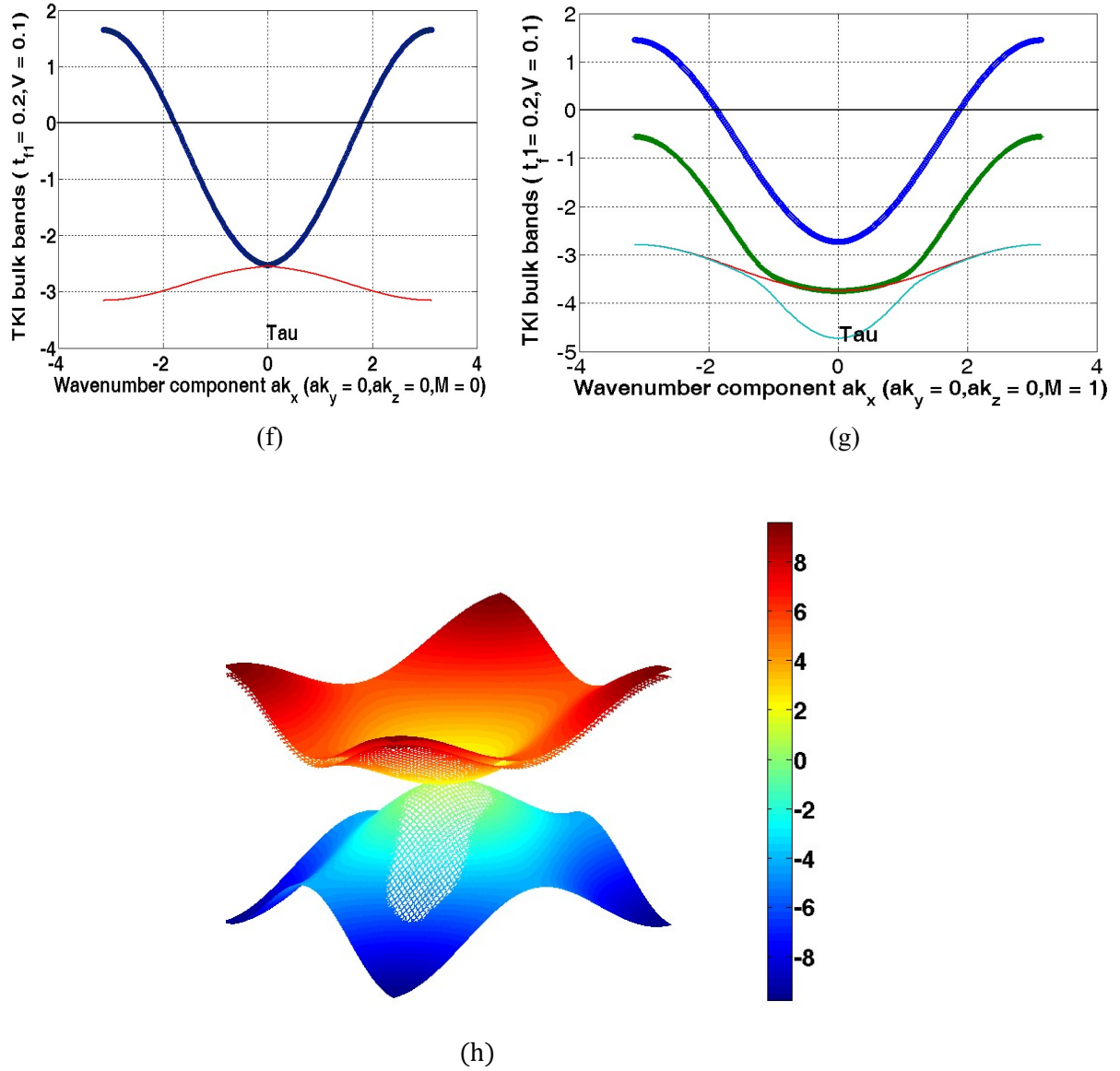


Figure 1. (a) A diagrammatic representation of SmB_6 crystal structure. The Sm ions are located at the corners and the B_6 octahedron at the center of the cubic lattice. (b), (c), (d) The plots of the bulk band energies (Eq. (6)) of the present system in the bulk insulating phase. The numerical values of the parameters used in the plots are $t_{d_1} = 1$, $t_{f_1} = -0.5$, $t_{d_2} = 0.01$, $t_{f_2} = 0.01$, $t_{d_3} = 0.001$, $t_{f_3} = 0.001$, $\epsilon_f = -0.02$, $V = V = 0.8$, $b = 0.9899$, $\mu = 0$, and $M \neq 0$. In Figures (e) and (f), however, $M = 0$. The Figures (f) and (g) show metallicity as $t_{f_1} > 0$. In Figure (g), $M \neq 0$. In Figure (h) we have 3D representation of all the four bands. The Fermi energy is represented by the horizontal solid line.

The bulk eigenstates corresponding to the eigenvalues in (6) are given by

$$|u_{n,k}\rangle = \frac{1}{N_n^{1/2}} \begin{pmatrix} 1 \\ -\frac{\vartheta_z}{A} \\ \frac{2M\vartheta_z}{B_n(k)} \\ -\frac{C_n(k)}{AB_n(k)} \end{pmatrix}, n=1, 2,3,4, A = (\vartheta_x - i\vartheta_y) \quad (7)$$

$$B_n(k) = (\vartheta_x^2 + \vartheta_y^2 + \vartheta_z^2) - (E_n - \widetilde{E}_k^d(\mu, k) + M)(E_n - \widetilde{E}_k^f(\mu, k)), \quad (8)$$

$$C_n(k) = (E_n - \widetilde{E}_k^d(\mu, k) + M) \vartheta_z^2 + (E_n - \widetilde{E}_k^d(\mu, k) - M)(\vartheta_x^2 + \vartheta_y^2) \\ + ((E_n - \widetilde{E}_k^d(\mu, k))^2 - M^2) (E_n - \widetilde{E}_k^f(\mu, k)), \quad (9)$$

$$N_n = (1 + \frac{\vartheta_z^2}{A^*A} + \frac{4M^2\vartheta_z^2}{B_n^2(k)} + \frac{C_n^2(k)}{A^*AB_n^2(k)}). \quad (10)$$

We now calculate here the intrinsic anomalous Hall conductivity (AHC)/Chern number(\mathcal{C}) to show that the system is in the quantum anomalous Hall (QAH) phase when $M \neq 0$. The expression of AHC is $\sigma_{AH} = -(\frac{e^2}{h}) \sum_j \int_{BZ} \frac{d^2k}{(2\pi)^3} g(E_j(k) - \mu) \Omega_j^z(k)$, where μ is the chemical potential of the fermion number, j is the occupied band index, $g(E_j(k) - \mu)$ is the Fermi-Dirac distribution and $\Omega_j^z(k)$ is the z -component of the Berry curvature (BC) for the j th band. To obtain AHC, we calculate BC using the Kubo formula

$$\Omega_j^z(k) = -2 \hbar^2 [Im \sum_{i \neq j} (E_j(k) - E_i(k))^{-2} \langle j, k | \widehat{v}_x | i, k \rangle \langle i, k | \widehat{v}_y | j, k \rangle]. \quad (11)$$

Here \mathbf{k} is the Bloch wave vector, $E_j(\mathbf{k})$ is the band energy, $|j, \mathbf{k}\rangle$ are the Bloch functions of a single band. The operator \widehat{v}_j represents the velocity in the j direction. For a system in a periodic potential and its Bloch states as the eigenstates, in view of the Heisenberg equation of motion $i\hbar \frac{d\widehat{x}}{dt} = [\widehat{x}, \widehat{H}]$, the identity $\langle m, \mathbf{k}' | \widehat{v}_\alpha | n, \mathbf{k} \rangle = (\frac{1}{\hbar}) (E_j(\mathbf{k}') - E_i(\mathbf{k})) \langle i, \mathbf{k}' | \frac{\partial}{\partial k_\alpha} | j, \mathbf{k} \rangle$ is satisfied. Upon using this identity, we obtain AHC in the zero temperature limit as $\sigma_{AH} = C (\frac{e^2}{h})$ where $C = \sum_j C_j$, $C_j = \int \int_{BZ} \Omega_j^z(k) \frac{d^2k}{(2\pi)^2}$. The z -component of the Berry-curvature(BC) is

$$\Omega_j^z(k) = \sum_j \left(\frac{\partial A_{j,y}}{\partial k_x} - \frac{\partial A_{j,x}}{\partial k_y} \right) = -2 \sum_j Im \left\langle \frac{\partial u_{j,k}}{\partial k_x} \middle| \frac{\partial u_{j,k}}{\partial k_y} \right\rangle \quad (12)$$

where $|u_{j,k}\rangle = |j, k\rangle$. The vector potential $A_j(\mathbf{k})$ is the Berry connection and $\nabla_{\mathbf{k}} \times A_j(\mathbf{k}) = \Omega_j(\mathbf{k})$ is the Berry curvature (BC). We use the results presented in Eq. (7) to calculate BC. The high symmetry points (HSPs) of the bulk Brillouin zone (BZ) are given above. Upon considering these points and the eigenvectors of the bulk system in (7), in line with the bulk-boundary

correspondence, the Berry curvature is calculated ensuring that all occupied levels are taken in. Next, upon integrating BC on a k-mesh-grid of the Brillouin zone, we calculate the intrinsic AHC. The contour plots of BC are given in Figure 2(a) and (b). The Chern number calculated in the two cases are **(a)** $\mathcal{C} = -1.9937 \sim -2$, **(b)** $\mathcal{C} = 1.4954$. A positive (negative) Chern number implies that the unidirectional edge waves propagate clockwise (anti-clockwise) with respect to the z-axis. However, what about the non-integer value? Regardless of this contentious issue, we believe that our analysis provides a strong evidence for the fact that the system is in the QAH phase when $M \neq 0$.

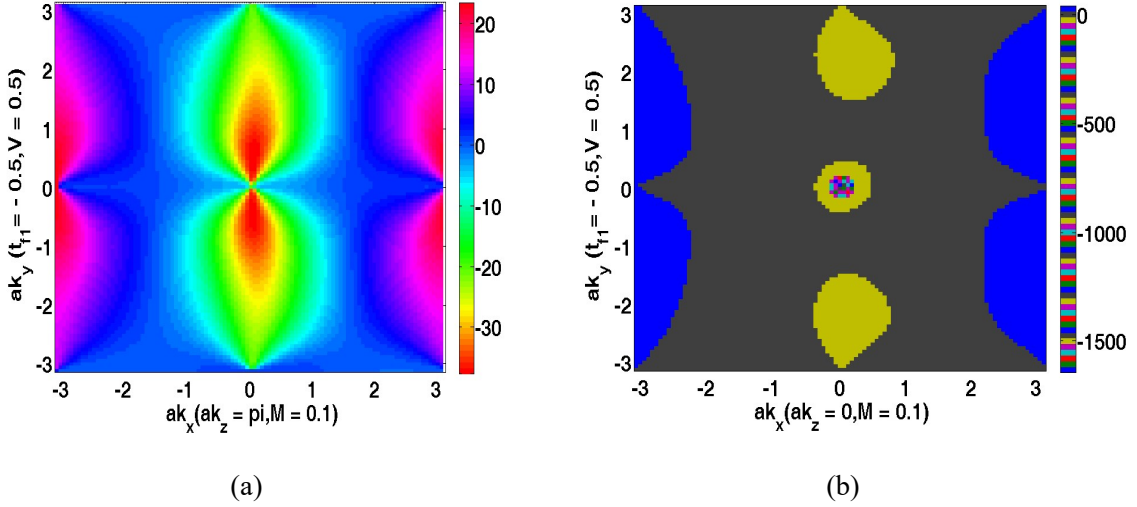


Figure 2. The contour plots of the Berry-curvature in the z-direction as a function of the dimension-less wave vector components ak_x and ak_y . The numerical values of the parameters used in the plots are $t_{d_1} = 1$, $t_{f_1} = -0.5$, $t_{d_2} = 0.1$, $t_{f_2} = 0.1$, $t_{d_3} = 0.01$, $t_{f_3} = 0.01$, $\epsilon_f = -0.02$, $V = 0.5$, $b = 0.9899$, $\mu = 0$, and $M = 0.10$. The Chern number calculated in the two cases are **(a)** $\mathcal{C} = -1.9937 \sim -2$, **(b)** $\mathcal{C} = 1.4954$.

3. Z_2 Invariant

For the purpose of calculating the Z_2 invariant when $M = 0$, we follow the well-known Fu and Kane [13] methodology based upon the eigenvalues of the parity operator. We summarize the procedure in brief after obtaining the surface state band spectrum in our slave-boson formalism. In order to obtain surface state Hamiltonian ($h_{\text{surface}}(k, \mu, b, M)$) we make the replacement $ak_z \rightarrow -ia \partial_z$ in (5) and look for states localized within the surface $z = 0$ of the form $\exp(-i\chi z)$. Furthermore, we seek such a value of the unknown wave number χ ($\chi = -iq$, $q > 0$) for which the exponential $\exp\left(-\frac{aqz}{a}\right) \ll 1$ for $z > 0$. For example, if we assume $aq \sim \pi$ the exponential $\exp\left(-\frac{aqz}{a}\right) \sim \exp(-30)$, i.e. vanishingly small, for $z \sim 50nm$ given that SmB₆ crystal structure with cubic lattice constant $a = 0.413$ nm (Figure 1(a)). Therefore, $\chi = -iq$, $q > 0$ ensures a decaying term for $z > 0$ in the surface states. Upon defining

$$\epsilon_0(k, \mu, b) = \frac{\widetilde{E}_k^d(\mu, k) + \widetilde{E}_k^f(\mu, b, k)}{2}, \epsilon(k, \mu, b) = \frac{\widetilde{E}_k^d(\mu, k) - \widetilde{E}_k^f(\mu, b, k)}{2}, \vartheta_{z0} = 2Vb \sin aq, \quad (13)$$

in the basis $(d_{k,\uparrow} \ bc_{k,\downarrow} \ d_{k,\downarrow} \ bc_{k,\uparrow})^T$, the surface state Hamiltonian appears as

$$h_{\text{surface}}(k, \mu, b, M) = (\epsilon_0(k, \mu, b))\sigma_0 \otimes \tau_0 - \vartheta_x \sigma_x \otimes \tau_x - \vartheta_y \sigma_y \otimes \tau_y + \epsilon(k, \mu, b) \sigma_0 \otimes \tau_z \\ + \left(\frac{M}{2}\right) (\sigma_x + \sigma_z) \otimes \tau_z + \left(\frac{1}{2}\right) [-i \vartheta_{z0} (\sigma_x + i\sigma_y) \otimes \tau_z + i \vartheta_{z0} (\sigma_x - i\sigma_y) \otimes \tau_x], \quad (14)$$

The Pauli matrices σ and τ are acting in the space of bands that give rise to Kramers degeneracy (see Figure 3 below). On a quick side note, it is perhaps worth mentioning that, for $M=0$ and $aq \sim \pi$, the Hamiltonian above could be written as

$$h_{\text{surface}}(k, \mu, b, M=0) = \begin{pmatrix} \mathfrak{h}_+ = \mathfrak{h}(k_x, k_y, q, \mu, b) & 0 \\ 0 & \mathfrak{h}_- = \mathfrak{h}^*(-k_x, -k_y, q, \mu, b) \end{pmatrix} \quad (15)$$

where $\mathfrak{h}_+ = (\epsilon(k, \mu, b))\tau_0 + \mathbf{n}(k_x, k_y, b) \cdot \boldsymbol{\tau}$, the two blocks $(\mathfrak{h}_+, \mathfrak{h}_-)$, characterized by the pseudo

-spin indices $(+, -)$, are related to each other by time reversal symmetry (TRS) for $M=0$, and $\mathbf{n}(k_x, k_y, q, b) = (-\vartheta_x, -\vartheta_y, \epsilon_0(k_x, k_y, \mu, b))$. Equation (15) corresponds to Qi-Wu-Zhang (QWZ) model[31-33]. As shown by these authors, the situation corresponds to the quantum spin Hall (QSH) state, for the spin Hall conductance of $\mathfrak{h}(k_x, k_y, q, \mu, b)$ and $\mathfrak{h}^*(-k_x, -k_y, q, \mu, b)$ are not zero but the net Hall conductance of the system described by Eq.(13) is zero. We shall, however, assume $aq \sim 1$ for the graphical representations and in section 3 below.

The assumption also ensures that $\exp\left(-\frac{aqz}{a}\right) \ll 1$ for $z > 0$.

The eigenvalues E_n ($n = 5, 6, 7, 8$) of $h_{\text{surface}}(k, \mu, b)$ in (14) is given by a quartic $E_n^4 + a E_n^3 + b E_n^2 + c E_n + d = 0$. The coefficients (a, b, c, d) are given by $a = -2(\widetilde{E}_k^d(\mu, k) + \widetilde{E}_k^f(\mu, b, k))$, $b = \{(\widetilde{E}_k^d(\mu, k) + \widetilde{E}_k^f(\mu, b, k))^2 - M^2 + 2C^2\}$, $C^2 = (\widetilde{E}_k^d(\mu, k) \times \widetilde{E}_k^f(\mu, b, k) - \vartheta_{z0}^2 + (\vartheta_x^2 + \vartheta_y^2))$, $c = \{M^2 \widetilde{E}_k^f(\mu, b, k) - C^2(\widetilde{E}_k^d(\mu, k) + \widetilde{E}_k^f(\mu, k, b))\}$, $d = -M^2 \times \widetilde{E}_k^f(\mu, b, k) + C^4 - 4 \vartheta_{z0}^2 (\vartheta_x^2 + \vartheta_y^2)$. In view of the Ferrari's solution of a quartic equation, we find the roots as

$$E_n(s, \sigma, k, b, M) = \sigma \sqrt{\frac{\eta_0(k)}{2}} - \frac{a}{4} + s \left(b_0(k) - \left(\frac{\eta_0(k)}{2}\right) + \sigma c_0(k) \sqrt{\frac{2}{\eta_0(k)}} \right)^{\frac{1}{2}}, \quad (16)$$

where $\sigma = \pm 1$ is the spin index and $s = \pm 1$ is the band-index. The functions appearing in Eq. (16) are given by

$$\eta_0(k) = \frac{2b_0(k)}{3} + (\Delta(k) - \Delta_0(k))^{\frac{1}{3}} - (\Delta(k) + \Delta_0(k))^{\frac{1}{3}}, \quad \Delta_0(k) = \left(\frac{b_0^3(k)}{27} - \frac{b_0(k)d_0(k)}{3} - c_0^2(k)\right), \quad (17)$$

$$\Delta(k) = \left(\frac{2}{729} b_0^6 + \frac{4d_0^2 b_0^2}{27} + c_0^4 - \frac{d_0 b_0^4}{81} - \frac{2b_0^3}{27} + \frac{2c_0^2 b_0 d_0}{3} + \frac{d_0^3}{27}\right)^{1/2}, \quad b_0(k) = \left\{\frac{3a^2 - 8b}{16}\right\}, \quad (18)$$

$$c_0(k) = \left\{\frac{-a^3 + 4ab - 8c}{32}\right\}, \quad d_0(k) = \frac{-3a^4 + 256d - 64ac + 16^2 b}{256}. \quad (19)$$

We have plotted the surface state energy spectra (SSES) given by Eq. (16), as well as the bulk band spectra, as function of the dimensionless wave vector component ak_x in Figures 3. Since the surface state bands E_n ($n = 6,7$) in 3(a) and E_n ($n = 7$) in 3(b) are partially empty, the surface state will be metallic. The curves E_n ($n = 6,7$) in 3(a) display the band-inversion. The Fermi energy is represented by the horizontal solid line. The numerical values of the parameters used in the plots are $t_{d_1} = 1$, $t_{f_1} = -0.5$, $t_{d_2} = 0.1$, $t_{f_2} = 0.1$, $t_{d_3} = 0.01$, $t_{f_3} = 0.01$, $\epsilon_f = -0.02$, $V = 0.5$, $b = 0.9899$, $\mu = 0$, and $M = 0$. In both the figures, t_{f_1} is negative and, therefore, the figures correspond to the insulating bulk. In Figure 3(b), there is a Kramers degeneracy at $ak_x = 0$, similar to what was reported in ref. [35]. The Dirac-cone feature (DCF) of SSES connecting the valence band with the conduction band has been observed in several experiments. These are reported earlier, such as the DCF observed by scanning-tunneling microscopy [36,37], angle-resolved photoemission spectroscopy (ARPES)[38,39], the circular dichroism ARPES[40], and so on. This feature is absent here as the linearization of the Hamiltonian matrix (5) has not been carried out about a Dirac point. However, we do observe that the states corresponding to $ak = (\pm 1, 0)$ in Figure 3 are degenerate and the Fermi energy(represented by the horizontal solid lines above) intersects the surface state bands in the same BZ only once. Furthermore, they satisfy the condition $ak + aG = -ak$ where aG is a reciprocal lattice vector. For example, when $ak =$

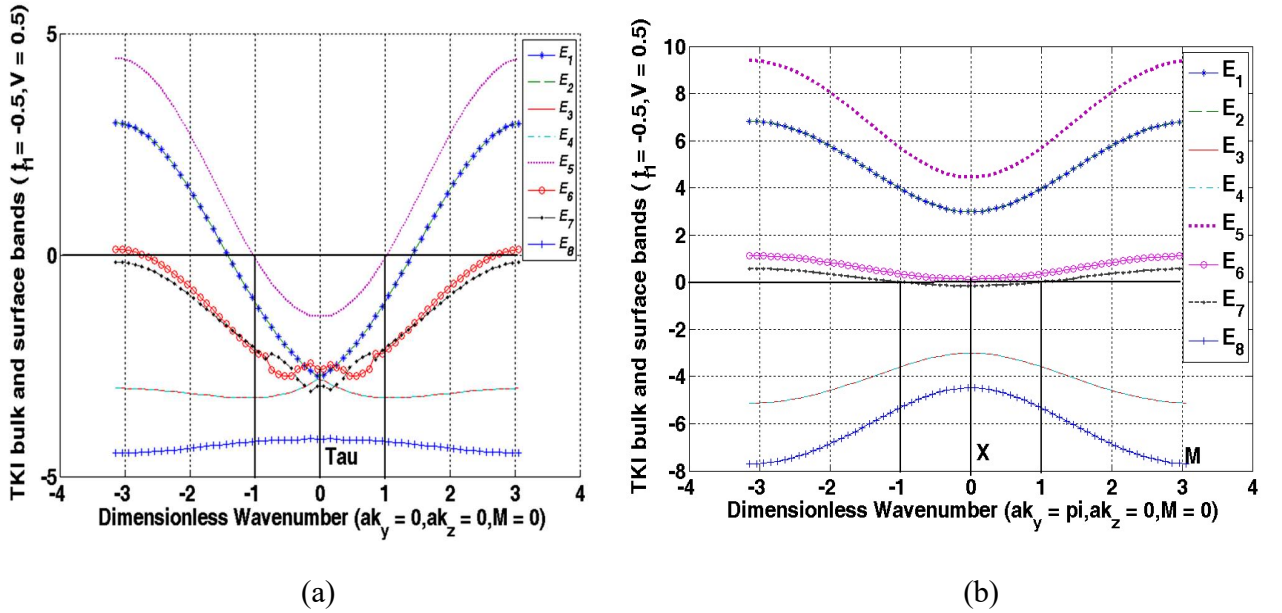


Figure 3. (a), (b) The plots of the bulk and surface band energies (Eq. (6), and Eq. (16)) of the system in the bulk insulating phase. The numerical values of the parameters used in the plots are $t_{d_1} = 1$, $t_{f_1} = -0.5$, $t_{d_2} = 0.1$, $t_{f_2} = 0.1$, $t_{d_3} = 0.01$, $t_{f_3} = 0.01$, $\epsilon_f = -0.02$, $V = 0.8$, $b = 0.9899$, $\mu = 0$, and $M = 0$. The Fermi energy is represented by the horizontal solid line.

$(\pm 1, 0)$ and $aG = (\mp 2, 0)$. Obviously, $ak = (\pm 1, 0)$ are the time reversal invariant momenta (TRIM). Since there is odd number of pair intersections, perhaps the surface state is topologically

non-trivial. This, most certainly, is not a conclusive evidence. However, the graphical representations (in Figure 3) do indicate that the system is a topological insulator (TI) for $M = 0$. We seek the corroboration of the non-triviality by the analysis given below.

The appearance of topologically-protected surface states is the physical consequence of the nontriviality mentioned above. Now the time reversal (TR) operator for a spin 1/2 particle is $\Theta = I^{2 \times 2} \otimes \tau^y K$. The operator K stands for the complex conjugation. The inversion symmetry (IS) operator, on the other hand, is constructed as $\Pi = I^{2 \times 2} \otimes \tau^z$. The τ^j are Pauli matrices on two-dimensional spin space. The Hamiltonian under consideration, for $M = 0$, preserves the time reversal (TRS) and inversion symmetries (IS). It can be easily shown that $\langle \Theta \psi | \Theta \varphi \rangle = \langle \varphi | \psi \rangle$ taking eigenstate of the z-component of the spin operator $I^{2 \times 2} \otimes \tau^z$ as the basis. Also, $\Theta \gamma^0 \Theta^{-1} = \gamma^0$, $\Theta \gamma^1 \Theta^{-1} = -\gamma^1$, and $\Theta \gamma^j \Theta^{-1} = \gamma^j$, where $j = 2, 3, 5$. Similarly, $\Pi \gamma^0 \Pi^{-1} = \gamma^0$, $\Pi \gamma^j \Pi^{-1} = -\gamma^j$ ($j = 1, 2$), and $\Pi \gamma^k \Pi^{-1} = \gamma^k$ ($k = 3, 5$). Since only γ^0, γ^3 , and γ^5 are even under time reversal and inversion, at a time reversal invariant momentum (TRIM) K_i where the system preserves both TR and IS, the Hamiltonian (5) will have the following form:

$$h_{\text{surface}}^{BHZ}(k = K_i, M = 0) = \left[\frac{\widetilde{E}_k^d(\mu, k) + \widetilde{E}_k^f(\mu, b, k)}{2} \mathbb{I} + \frac{\widetilde{E}_k^d(\mu, k) - \widetilde{E}_k^f(\mu, b, k)}{2} \gamma^0 + 2Vb \sin ak_{z0} \gamma^0 \gamma^3 \right]. \quad (20)$$

The eigenvalues of Π, γ^0 and $\gamma^0 \gamma^3$ are ± 1 (multiplicity 2). The eigenvectors corresponding to the eigenvalues $+1$ and -1 of the parity operator, respectively, are $|+\rangle = (1/\sqrt{2})(1 \ 0 \ 1 \ 0)^T$ and $|-\rangle = (1/\sqrt{2})(0 \ -1 \ 0 \ -1)^T$. These are the relevant eigenstates. It is easy to see that

$$\begin{aligned} \langle + | h_{\text{surface}}^{BHZ}(k = K_i, M = 0) | + \rangle &= \widetilde{E}_k^d(\mu, k) + 2Vb \sin ak_{z0} = E_+, \\ \langle - | h_{\text{surface}}^{BHZ}(k = K_i, M = 0) | - \rangle &= \widetilde{E}_k^d(\mu, k) - 2Vb \sin ak_{z0} = E_-. \end{aligned} \quad (21)$$

Obviously enough, $E_- < E_+$. Thus, the occupied state corresponds to the parity eigenvalue -1 . Since the Z_2 invariant is determined by the parity eigenvalue of the occupied state, the compound SmB_6 unequivocally is an STI. This is in disagreement with what had been reported in refs.[7,8].

4. Discussion and concluding remarks

As already stated, the strong correlation effects and diverse surface conditions make a generic TKI system extremely complicated and almost a Gordian knot. Despite this, as we have seen above, our analysis was able to show that SmB_6 is an STI. However, there is a caveat which concerns the fact that we have assumed $aq \sim 1$. Regarding this we have no clue except that, whatever be the assumption, it has to ensure that $\exp\left(-\frac{aqz}{a}\right) \ll 1$ for $z > 0$. This aside, our analysis was not able to capture the fact that there should be a surface Dirac cone at $k = 0$ (as in ref.[35]) in Figure 3 for $M = 0$. Another point is that Dirac cones must exist in three different TRIMs of the surface BZ [41]. The reason for the absence of both is that the linearization of the Hamiltonian matrix (5) has not been carried out about a Dirac point. For $M \neq 0$ (Figures 1 and 2),

by calculating BC and the Chern number we have been able to show that the system is likely to correspond to QAH state. The problem needs an extensive investigation introducing an additional term $h_z = \left[\left(\frac{1}{2} \right) \left(-\alpha_0 \sin(k_y a) \right) \sigma_x \otimes (\tau_z + \tau_0) + \left(\frac{1}{2} \right) \alpha_0 \sin(k_x a) \sigma_y \otimes (\tau_z + \tau_0) \right]$, which is the Rashba spin-orbit coupling (RSOC) between the d -electrons, in Eq. (5). Here α_0 stands for the strength of RSOC. These are some of the essential points of the present report. The Rashba coupling can arise in a system due to the proximity of material lacking in the structural inversion symmetry. In view of the spin-polarized ARPES measurements which appear to confirm the surface helical spin texture [42,43], it would be interesting to see how does surface state react to Rashba splitting.

There are many other complications [44-50] to bring home the point that the system needs concerted investigations. In fact, we are presently working on one of the several issues [44-50]. This is as follows: Since we have considered surface state, the next step forward is an investigation on the Kondo break down[44]. There are other contentious issues, such as the Hermiticity of an open system is universally lost as the system always involves certain degrees of gain and loss. The ubiquitous electron-electron, electron-impurity, and electron-photon scatterings in an electronic system are responsible for this loss/gain. It is hoped that these issues will motivate the condensed matter physics community to delve deeper into the problem.

In conclusion, looking at the controversies and the possibilities [7-9,42-50], it is anybody's guess that there are many unsettled issues. Unless other TKI candidates are discovered and thoroughly studied, it is perhaps difficult to achieve enhancement in the current understanding of strongly correlated topological insulators. In this backdrop, it is pertinent to make an attempt to investigate thoroughly what exactly are the physical explanation of the issues involved. In a future communication, as we already stated, we undertake a part of this demanding task.

References

- 1 D. J. Kim, S.Thomas.; T. Grant, J. Botimer, Z. Fisk, J.Xia, Sci. Rep., 3, 3150(2013).
- 2 .M.Dzero, K Sun, V. Galitski, P. Coleman, Phys. Rev. Lett. 2010, 104, 106408(2010); *ibid* Rev. B 2012, 85, 045130 (2012).
- 3.Udai Prakash Tyagi, Kakoli Bera and Partha Goswami, On Strong f -Electron Localization Effect in a Topological Kondo Insulator, *Symmetry*,13(12), 2245 (2021); <https://doi.org/10.3390/sym13122245>.
4. S. Wolgast, C. Kurdak, K. Sun, J. W. Allen, D.-J. Kim, and Z. Fisk, Phys. Rev. B 88, 180405 (2013).
5. X. Zhang, N. P. Butch, P. Syers, S. Ziemak, R. L. Greene, and J. Paglione, Phys. Rev. X 3, 011011 (2013).
6. D. J. Kim, J. Xia, and Z. Fisk, Nat. Mater. 13, 466 (2014).
7. A. P. Sakhya and K.B. Maiti , Scientific Reports volume 10, Article number: 1262 (2020).
8. P. Hlawenka, K. Siemensmeyer, E. Weschke, *et al.*, Samarium hexaboride is a trivial surface conductor. *Nat Commun* 9, 517 (2018). <https://doi.org/10.1038/s41467-018-02908-7>

9. P. K. Biswas, M. Legner, G. Balakrishnan, M. C. Hatnean, M. R. Lees, D. M. Paul, E. Pomjakushina, T. Prokscha, A. Suter, T. Neupert, et al., *Phys. Rev. B* 95, 020410 (2017).
10. M. Legner, *Topological Kondo insulators: materials at the interface of topology and strong correlations* (Doctoral Thesis), ETH Zurich Research Collection (2016). Link: <https://www.research-collection.ethz.ch/bitstream/handle/20.500.11850/155932/eth-49918-02.pdf?isAllowed=y&sequence=2>.
11. A. Sharma, H. Yan, L. Zhang, X. Sun, X. B. Liu, Y. Lu, Y. Highly enhanced many-body interactions in anisotropic 2D semiconductors. *Accounts of Chemical Research*. 2018;51(5):1164–1173. doi: 10.1021/acs.accounts.7b00504.
12. Y. J. Jin, R. Wang, B. W. Xia, B. B. Zheng, and H. Xu, Three-dimensional quantum anomalous Hall effect in ferromagnetic insulators, *Phys. Rev. B* 98, 081101(R) (2018).
13. L. Fu, C.L. Kane.: Time reversal polarization and a Z_2 adiabatic spin pump. *Phys. Rev. B* 74, 195312 (2006); L. Fu, C. L. Kane, and E.J. Mele: Topological insulators in three dimensions. *Phys. Rev. Lett.* 98, 106803 (2007); C. L. Kane, and E.J. Mele: Z_2 Topological Order and the Quantum Spin Hall Effect. *Phys. Rev. Lett.* 95, 146802 (2005).
14. S. Sajad Dabiri, Hosein Cheraghchi, Ali Sadeghi, Light-induced topological phases in thin films of magnetically doped topological insulators *Physical Review B* 103, 205130 (2021); Haowei Xu, Jian Zhou, Ju Li, Light-induced quantum anomalous Hall effect on the 2D surfaces of 3D topological insulators, *Advanced Science*, 2101508 (2021).
15. W. Zhu, M. Umer, and J. Gong, *Phys. Rev. Research* 3, L032026 (2021).
16. L. Zhou, C. Chen, and J. Gong, *Phys. Rev. B* 94, 075443 (2016).
17. H. Hubener, M. A. Sentef, U. De Giovannini, A. F. Kemper, and A. Rubio, *Nat. Commun.* 8, 13940 (2017).
18. D. Zhang, H. Wang, J. Ruan, G. Yao, and H. Zhang, *Phys. Rev. B* 97, 195139 (2018).
19. H. Liu, J.-T. Sun, and S. Meng, *Phys. Rev. B* 99, 075121 (2019).
20. L. Li, C. H. Lee, and J. Gong, *Phys. Rev. Lett.* 121, 036401 (2018).
21. X. Liu, P. Tang, H. Hubener, U. De Giovannini, W. Duan, and A. Rubio, arXiv preprint arXiv:2106.06977 (2021).
22. F. Qin, R. Chen, and H.-Z. Lu, *J. Phys. Condens. Matter* 34, 225001 (2022).
23. J. W. McIver, B. Schulte, F.-U. Stein, T. Matsuyama, G. Jotzu, G. Meier, and A. Cavalleri, Light-induced anomalous hall effect in graphene, *Nature Physics* 16, 38 (2019).
24. B. K. Wintersperger, C. Braun, F. N. Unal, A. Eckardt, M. D. Liberto, N. Goldman, I. Bloch, and M. Aidelsburger, Realization of an anomalous floquet topological system with ultracold atoms, *Nature Physics* 16, 1058 (2020).
25. C. S. Afzal, T. J. Zimmerling, Y. Ren, D. Perron, and V. Van, Realization of anomalous floquet insulators in strongly coupled nanophotonic lattices, *Phys. Rev. Lett.* 124, 253601 (2020).
26. H. Sambe, Steady states and quasi-energies of a quantum mechanical system in an oscillating field, *Phys. Rev. A* 7, 2203 (1973).
27. A. A. Pervishko, D. Yudin, and I. A. Shelykh, Impact of high-frequency pumping on anomalous finite-size effects in three-dimensional topological insulators, *Phys. Rev. B* 97, 075420 (2018).
28. R. Chen, B. Zhou, and D.-H. Xu, Floquet Weyl semimetals in light-irradiated type-II and hybrid line node semimetals, *Phys. Rev. B* 97, 155152 (2018).; R. Chen, D.-H. Xu, and B. Zhou, Floquet topological insulator phase in a Weyl semimetal thin film with disorder, *Phys. Rev. B* 98, 235159 (2018).
29. N. Goldman and J. Dalibard, Periodically Driven Quantum Systems: Effective Hamiltonians and Engineered Gauge Fields, *Phys. Rev. X* 4, 031027 (2014); A. Eckardt and E. Anisimovas, High-frequency approximation for periodically driven quantum systems from a Floquet-space perspective, *New J. Phys.* 17, 093039 (2015).

30. Y. Yang, Z. Xu, L. Sheng, B. Wang, D. Y. Xing, and D. N. Sheng, Time-reversal-symmetry-broken quantum spin Hall effect, *Phys. Rev. Lett.* 107, 066602(2011).
31. Y. Zhang, C.-X. Liu, X.-L. Qi, X. Dai, Z. Fang, and S.-C. Zhang, Topological insulators in Bi_2Se_3 , Bi_2Te_3 and Sb_2Te_3 with a single Dirac cone on the surface, *Nat. Phys.* 5 438 (2009).
32. X.-L. Qi, Y.-S. Wu, and S.-C. Zhang, Topological quantization of the spin hall effect in two-dimensional paramagnetic semiconductors, *Phys. Rev. B* 74, 085308 (2006).
33. X.-L. Qi and S.-C. Zhang, Topological insulators and superconductors, *Reviews of Modern Physics* 83, 1057 (2011).
34. B. A. Bernevig, T. L. Hughes, and S.-C. Zhang: *Science* **314**, 1757 (2006).
35. There should be a surface Dirac cone or at least a Kramers degeneracy at $k=0$. See for comparison the Dirac cone topological surface states at TRIMS calculated by DFT [F. Lu](#), [J. Zhou Zhao](#), [H. Weng](#), [Z. Fang](#), [Xi Dai](#) *Phys. Rev. Lett.* 110, 096401 (2013).
36. W. Ruan, C. Ye, M. Guo, F. Chen, X. Chen, G.-Ming Zhang, and Y. Wang, *Phys. Rev. Lett.* 112, 136401 (2014).
37. S. Röblier, T.-Hwan Jang, D.-Jeong Kim, and S. Wirth, *Proc. Natl. Acad. Sci. U.S.A.*, 111 (13) 4798 (2014). <https://doi.org/10.1073/pnas.1402643111>.
38. Neupane, M., Alidoust, N., Xu, S.Y. *et al.* Surface electronic structure of the topological Kondo-insulator candidate correlated electron system SmB_6 . *Nat Commun* **4**, 2991 (2013). <https://doi.org/10.1038/ncomms3991>.
39. Jiang, J., Li, S., Zhang, T. *et al.* Observation of possible topological in-gap surface states in the Kondo insulator SmB_6 by photoemission. *Nat Commun* **4**, 3010 (2013). <https://doi.org/10.1038/ncomms4010>.
40. Xu, N., Biswas, P., Dil, J. *et al.* Direct observation of the spin texture in SmB_6 as evidence of the topological Kondo insulator. *Nat Commun* **5**, 4566 (2014). <https://doi.org/10.1038/ncomms5566>.
41. Feng Lu, *et al.*, *Phys. Rev. Lett.* 110, 096401 (2013)
42. N. Xu, P.K. Biswas, J.H. Dil, G. Landolt, S. Muff, C.E. Matt, X. Shi, N.C. Plumb, M. Radović, E. Pomjakushina, K. Conder, A. Amato, S.V. Borisenko, R. Yu, H.-M. Weng, Z. Fang, X. Dai, J. Mesot, H. Ding, and M. Shi, *Nat. Commun.* 5, 4566 (2014).
43. S. Suga *et al.*, *J. Phys. Soc. Jpn* 83, 014705 (2014).
44. V. Alexandrov, P. Coleman, O. Erten, *Phys. Rev. Lett.* 114, 177202 (2015).
45. S. Sen *et al.*, *Physical Review Research* 2, 033370 (2020).
46. Knolle, J. & Cooper, N. R., *Phys. Rev. Lett.* 118, 096604 (2017).
47. Erten, O., Chang, P.-Y., Coleman, P. & Tsvelik, A. M., *Phys. Rev. Lett.* 119, 057603 (2017).
48. Chowdhury, D., Sodemann, I. & Sentil, T., *Nat. Commun.* 9, 1766 (2018).
49. Shen, H. and Fu, L., *Phys. Rev. Lett.* 121, 026403 (2018).
50. D. Chowdhury, I. Sodemann, and T Sentil, *Nat. Commun.* 9, 1766 (2018).

Statement Regarding Data Analyzed

All data used or analyzed during this study are included in this article.